View metadata, citation and similar papers at core.ac.uk
brought to you by CORE
provided by Repositorio Institucional de la Universidad de Oviedo

arXiv:0907.2678v1 [cond-mat.mes-hall] 15 Jul 2009

Magnetic properties of small Pt-capped Fe, Co and Ni clusters: A density functional theory study

Sanjubala Sahoo,* Alfred Hucht, Markus E. Gruner, and Peter Entel

Physics Department, University of Duisburg–Essen, Lotharstr. 1, D-47048 Duisburg, Germany

Andrei Postnikov

LPMD, Paul Verlaine University – Metz, 1 Bd Arago, F-57078 Metz, France

Jaime Ferrer and Lucas Fernández-Seivane

Departamento de Física, Universidad de Oviedo, 33007 Oviedo, Spain

Manuel Richter and Daniel Fritsch

IFW Dresden e.V., Helmholtzstr. 20, P.O. Box 270116, D-01171 Dresden, Germany

Shreekantha Sil

Department of Physics, Visva Bharati University, Santiniketan, 731235 West Bengal, India

Abstract

Theoretical studies on M_{13} (M = Fe, Co, Ni) and $M_{13}Pt_n$ (for n = 3, 4, 5, 20) clusters including the spin-orbit coupling are done using density functional theory. The magnetic anisotropy energy (MAE) along with the spin and orbital moments are calculated for M_{13} icosahedral clusters. The angle-dependent energy differences are modelled using an extended classical Heisenberg model with local anisotropies. From our studies, the MAE for Jahn-Teller distorted Fe_{13}, Mackay distorted Fe_{13} and nearly undistorted Co_{13} clusters are found to be 322, 60 and 5 μeV/atom, respectively, and are large relative to the corresponding bulk values, (which are 1.4 and 1.3 μeV/atom for bcc Fe and fcc Co, respectively.) However, for Ni_{13} (which practically does not show relaxation tendencies), the calculated value of MAE is found to be 0.64 μeV/atom, which is approximately four times smaller compared to the bulk fcc Ni (2.7 μeV/atom). In addition, MAE of the capped cluster ($Fe_{13}Pt_4$) is enhanced compared to the uncapped Jahn-Teller distorted Fe_{13} cluster.

PACS numbers: Valid PACS appear here

*Electronic address: sanjubala.sahoo@uni-due.de

I. INTRODUCTION

Density-functional theory (DFT) is an adequate tool to obtain useful information on the physical properties of small clusters. However, with respect to magnetic properties, the variations of magnetic moments with cluster size and morphology are often too obscure for establishing a clear trend (for example, see the behavior of the exchange coupling of free Fe clusters in [1, 2]). Still, certain general statements can be made. It may be safely concluded that the local magnetic moments in outer shells of clusters are enhanced, as compared to the interior of clusters or to the corresponding bulk crystal [3, 4, 5, 6]. This is a typical effect of reduced atomic coordination at the surface [7], well known from numerous experiments or calculations of magnetic slabs. Moreover, an analysis of cluster morphologies, by both experiment and theory [8, 9, 10, 11, 12, 13, 14, 15], reveals the importance of icosahedral-like structures, prohibited for bulk or surface phases. On the other hand, the diversity of cluster structures in combination with the surface enhancement of magnetic moments make clusters interesting model objects for tuning magnetic properties at the nanometer scale.

When addressing magnetic properties of clusters from the computational point of view at a realistic level, it is important to take into account two specific issues: (*i*) a possible non-collinear (NC) setting of magnetic moments (i.e., a smooth variation of magnetic density vector from point to point in space), and (*ii*) spin-orbit interaction (SOI), along with the existence of orbital moments. Both issues have a long record of incorporation into first-principles DFT calculations, and are internally related: They mix the spin-up and spin-down states and must be, in principle, treated alongside on equal footing (see, e.g., Refs. [16, 17] for a review). Discussing specifically DFT calculations for clusters, one notes certain technical difficulties in combining NC spin density with the SOI, which acted so far as a limiting factor on the number of calculations performed, and the size of clusters treated: Lack of symmetry, big effect of structure relaxation, slow convergence, large size of simulation cell around a free cluster. Moreover there is a conceptual problem of choosing a "correct" non-collinear solution among many apparently close metastable configurations. Different groups report very different results for the same systems (e.g., Refs. [18, 19, 20]), so that a preference of one or another result is not obvious. Therefore, not so much the size of cluster is a problem in itself, as the organization of a calculation in a way allowing to extract meaningful results, that is, clearly defining structural and magnetic models and carefully

analyzing their consequences.

A better understanding of the origins and details of large orbital magnetic moment as well as large MAE in clusters [21, 22] is demanding in order to manipulate materials for improving the technology like in magnetic data storage devices. Binary $3d$–$5d$ clusters can be a challenging material in this respect. For example, there are observations that $4d$ and $5d$ elements like Rh, Pt and Au, which are nonmagnetic in bulk phase, attain significant moments when alloyed with $3d$ transition metals like Fe, Co or Ni [23, 24, 25, 26].

In the present work, we analyze the effect of capping icosahedral clusters M_{13} of M = Fe, Co, and Ni with Pt atoms. Theoretically, there have been several studies on magnetic anisotropy for supported clusters [27, 28, 29, 30, 31, 32, 33], whereas studies on small free clusters are still limited [34, 35, 36, 37, 38]. The motivation for the present study is that icosahedral clusters for M_{13} are known to be very stable, [6, 12, 39] and the alloying of $3d$ transition metals with Pt results in large magnetic anisotropy as well as orbital moment. Hence, it is expected that the orbital and the spin moments of M_{13} clusters be strongly affected by capping with Pt.

Most of our DFT calculations have been done with the planewave code VASP (Vienna Ab-Initio Simulation Package) [40, 41, 42]. For test purposes and for validating the results of calculations on non-capped icosahedral clusters, we performed calculations also with a local-orbitals code, SIESTA (Spanish Initiative for Electronic Simulations with Thousands of Atoms) [43]. As the two methods are very different in what regards the technical implementation of the DFT calculation scheme, and both have been earlier used in calculations of magnetic clusters, their direct comparison might be of its own interest. In addition, few test calculations for the binary clusters were done using the all-electron local-orbital code FPLO (Full-Potential Local-Orbital scheme) [44]. In this respect, it is interesting to note that all-electron calculations confirm the results obtained with VASP and SIESTA.

The paper is organized as follows. Section II outlines the calculational methods and setup. Section III deals with the results for monometallic icosahedral clusters, notably comparison between VASP and SIESTA results. Section IV discusses the results for capped clusters, obtained with the VASP code. We have made a comparison between VASP and FPLO for one of the capped clusters. Conclusions are drawn in Section V.

II. COMPUTATIONAL METHODS

Most of the calculations have been performed with the VASP code [40, 41, 42] based on DFT and within the generalized gradient approximation (GGA). The parameters by Perdew are used for the exchange and correlation functional [45]. VASP uses the projector augmented wave (PAW) method [42, 46] and a planewave basis set. Periodic boundary conditions were imposed onto large enough cubic cells (with the edge of 15 Å for M_{13} clusters and 20 Å for $M_{13}Pt_n$ clusters) in order to sufficiently reduce the interaction between replicated cluster images. Only the Γ point was used for the Brillouin-zone sampling for the cluster calculations. A k-mesh of (11×11×11) is used for the bulk calculations to compute the equilibrium lattice constants in case of bcc Fe, fcc Ni and Co. The values for local magnetic moments correspond to the integration of continuous magnetization density over atom-centred spheres with radii of 1.302 Å (Fe, Co), 1.286 Å (Ni) and 1.455 Å (Pt). It is a well known fact that the magnetic anisotropy energy for cubic bulk transition metals, defined as the maximum energy difference, per atom, between different settings of the spin moment relative to the atoms framework, is of the order of 10^{-6} eV. Moreover, a special care is demanded for the study of the MAE in clusters because any slight error can accumulate and produce misleading results while dealing with energy differences of such a small scale. In order to calculate the magnetic anisotropy of M_{13} icosahedral clusters, we have used the energy convergence criterion for the self-consistency as 10^{-10} eV with a Gaussian half-width parameter of 0.01 eV for the discrete energy levels. A very high plane wave cutoff value of 1000 eV as well as a dense Fourier grid spacing of 0.04 Å in each of x, y and z directions is taken.

While relaxing the clusters using conjugate gradient algorithm, the same energy convergence criterion is used but a lower plane wave cut-off of 270 eV. The structural relaxation of clusters are done in the scalar relativistic mode. For the calculation of orbital moment and MAE, the SOI is treated as a perturbation in the scalar relativistic Hamiltonian. Benchmark calculations for some M_{13} clusters have also been done with the SIESTA code [43] within GGA, where the exchange and correlation functional is parameterized by Perdew, Burke and Ernzerhof [47]. It uses the norm-conserving pseudopotentials of Troullier and Martins [48]. The localized basis functions of "double-ζ with polarization orbitals" quality (and triple-ζ for $3d$ functions) have been constructed according to the standard scheme of

the SIESTA method [49], with the "Energy Shift" parameter of 0.01 Ry. The treatment of SOI was included as described by Fernandez-Seivane *et al.* [50]. In the SIESTA calculations, we used the atomic coordinates as relaxed by VASP. This allows for a direct comparison of non-collinear structures, spin and orbital moments. The standard representation of local magnetic moments in SIESTA is in terms of Mulliken populations of localized orbitals, that is a quite different definition from that used in VASP. For the sake of better comparison, we report in the following the magnetic moments as properties integrated over atom-centred spheres for both VASP and SIESTA.

TABLE I: Relaxed coordinates (Å) for Jahn-Teller distorted (JT) and Mackay transformed (MT) Fe_{13} clusters. See Fig. 1 for an illustration and labelling of atoms.

	Fe_{13}(JT)			Fe_{13}(MT)		
Atom Nr.	x	y	z	x	y	z
1	0.6764	−2.0818	−1.0306	0.0000	−1.2917	−2.0157
2	−0.6764	2.0818	1.0306	0.0000	1.2917	2.0157
3	0.0000	0.0000	−2.3361	0.0000	1.2916	−2.0157
4	0.0000	0.0000	2.3361	0.0000	−1.2916	2.0157
5	−0.6764	−2.0818	1.0306	−1.2917	−2.0157	0.0000
6	1.7709	−1.2866	1.0306	1.2916	−2.0157	0.0000
7	−1.7709	1.2866	−1.0306	−1.2916	2.0157	0.0000
8	0.6764	2.0818	−1.0306	1.2917	2.0157	0.0000
9	−1.7709	−1.2866	−1.0306	−2.0157	0.0000	−1.2917
10	2.1890	0.0000	−1.0306	2.0157	0.0000	−1.2916
11	−2.1890	0.0000	1.0306	−2.0157	0.0000	1.2916
12	1.7709	1.2866	1.0306	2.0157	0.0000	1.2917
13	0.0000	0.0000	0.0000	0.0000	0.0000	0.0000

Finally, several test calculations have been performed by a third method in order to confirm the presented results. These calculations are documented later in Section IV and have been carried out with the all-electron local-orbital code (FPLO 6.00-24) [44] in its cluster mode [51] using LSDA [52]. The valence basis comprised $3s3p3d$ $4s4p4d$ $5s$ states for $3d$-metals, while $5s5p5d$ $6s6p6d$ $7s$ states were used for Pt. The fully relativistic mode is employed here, where FPLO solves the four-component Dirac-Kohn-Sham equations including spin-orbit coupling (at the single electron level) in all orders [53]. Default settings were used for the other numerical parameters.

III. RESULTS FOR MONOMETALLIC ICOSAHEDRAL CLUSTERS M_{13}

In order to systematically pursue a search towards probable relaxation patterns from the ideal icosahedron (ICO) structure, we "drove" the structure along two different paths, which are known from previous studies [12, 54, 55, 56] and are likely to lead to different metastable arrangements. The structural relaxation of M_{13} clusters results in Jahn-Teller (JT) distortion as well as partially Mackay transformed (MT) clusters (Fe, Co, Ni), which is shown in Fig. 1 for the case of Fe_{13}. For the Fe_{13} cluster, the JT-distorted structure is by 123 meV/cluster, the MT cluster by 35 meV/cluster lower in energy compared to the energy of the ideal ICO, see also Ref. [12]. Only the Fe cluster exhibits the JT-distortion and the Mackay distortion as additional local minimum in the energy curve [54, 55], whereas Co and Ni show only a tendency for MT.

What we refer to in the following as the Jahn-Teller (JT) type distortion [58] is that which maintains the fivefold symmetry around one of the ICO axes; it allows a compression or tension of the cluster along this axis, possibly accompanied by a mutual opposite rotation of two pentagonal rings pierced by the axis in question.

The occurrence of the JT distortion originates from (accidental) quasi-degeneracy of the highest occupied molecular orbitals so that the system may lower its energy by level splitting arising from the induced distortion and corresponding redistribution of electrons. The partially Mackay distortion is of completely different origin since it is connected with the tendency of the magnetic Fe clusters to transform to the fcc cuboctahedron (CUBO) and by subsequent Bain like transformation to bcc Fe. Whereas for large Fe clusters, the JT distortion is no longer observed, we find in the simulations that the partially Mackay transformed cluster (which were denoted as shell-wise Mackay transformed cluster in [12, 56]) still corresponds to a metastable [59] (local energy minimum) state up to cluster sizes having 15 closed atomic shells (n) and magic atom numbers (N) defined by

$$N = \tfrac{1}{3}(10n^3 + 15n^2 + 11n + 3).$$

For the Fe_{13} cluster, the JT distortion corresponds to a compression of the cluster along the z- axis as depicted in Fig. 1, whereas we have chosen a different orientation for the MT cluster in the same figure (z-axis through mid-points of two opposite bonds) in order to illustrate its more cubic-like appearance. The relaxed atomic coordinates for the MT

TABLE II: The bond lengths in Å for relaxed Mackay transformed M_{13} clusters.

Bonds	Fe_{13}	Co_{13}	Ni_{13}
Centre-shell	2.394	2.33	2.321
24 ×	2.501	2.451	2.441
6 ×	2.583	2.447	2.439

and JT 13-atom Fe clusters are listed in Table I. For the JT-distorted Fe_{13} cluster, 10 of the peripheral atoms lie at a distance of 2.42 Å from centre, the other two atoms show an inward relaxation towards the centre and hence, remain at a distance of 2.34 Å from centre. A clear picture of the relaxation is shown in the left panel of Fig. 1, where the arrows associated with atoms on the top and bottom of the box face oppositely. The structural relaxation of the Fe_{13} cluster shown in the right panel in Fig. 1 corresponding to the partial Mackay transformation is the onset of the transformation from an ICO to CUBO, where the consecutive triangular facets of the ICO change to square facets of the CUBO, which can be described by a parameter s defined as the square of the ratio of the stretched to the unstretched edges being 1 and 2 for the ICO and CUBO, respectively. See [57] for the original explanation. It is well observed for multishell ICO-like Fe clusters [12, 56]. In our calculations, the relaxed Fe_{13} has $s = 1.07$; Co_{13} and Ni_{13} have $s \approx 1$, resulting in an almost ideal icosahedral like structure.

The peripheral bond lengths for the MT clusters (see Table II) can be arranged in groups: 6 of the 30 bonds being parallel to the cartesian axes (x: 5-6, 7-8; y: 1-3, 4-2; z: 9-11, 10-12; see Fig. 1 for the labeling of the atoms), the remaining 24 bond lengths are also listed in Table II. Remarkably, the distances of the 12 peripheral atoms to the central one are all identical.

The relaxed MT coordinates obtained with VASP have been used in the calculation by SIESTA, without further relaxation, in order to compare the resulting values of spin and orbital moments, and the non-collinearity. Table III compares the calculated results by the two methods for Fe_{13}(MT) and Co_{13} (MT) clusters. For both methods, the spin moments remain parallel (x- and y-components of the spin vectors are, at most, 0.001 μ_B, and are not shown in Table III). The orbital moments for MT distorted Fe_{13} obtained by both programs are directed towards the $z-$direction in the lower part of the cluster and are deviated "outwards" from the $z-$direction in the upper part, while for Co_{13}, they show

TABLE III: Spin and orbital moments of the relaxed Fe_{13} (MT) and Co_{13} clusters as calculated by VASP and SIESTA, for the initial [001] setting of spin direction. The x and y-components of the spin moment are < 0.001, hence not shown here. For SIESTA calculations, the values of spin moments are given in terms of Mulliken populations, the magnetic moments are in units of μ_B/atom.

	Vasp				Siesta			
				Fe_{13}				
Atom No.	L_x	L_y	L_z	S_z	L_x	L_y	L_z	S_z
1	0.00	-0.02	0.11	3.06	0.00	-0.01	0.09	3.43
2	0.00	0.02	0.12	3.06	0.00	0.01	0.09	3.43
3	-0.01	0.00	0.08	3.08	-0.01	0.00	0.08	3.43
4	0.01	0.00	0.08	3.08	0.01	0.00	0.08	3.44
5	0.00	0.00	0.07	3.10	0.00	0.00	0.06	3.44
6	0.00	0.00	0.07	3.10	0.00	0.00	0.06	3.44
7	0.00	0.00	0.07	3.10	0.00	0.00	0.06	3.44
8	0.00	0.00	0.07	3.10	0.00	0.00	0.06	3.44
9	0.01	0.00	0.08	3.08	0.01	0.00	0.08	3.44
10	-0.01	0.00	0.08	3.08	-0.01	0.00	0.08	3.44
11	0.00	0.02	0.11	3.05	0.00	0.01	0.09	3.43
12	0.00	-0.02	0.11	3.06	0.00	-0.01	0.09	3.43
13	0.00	0.00	0.05	2.70	0.00	0.00	0.03	2.75
				Co_{13}				
1	0.00	0.03	0.09	2.10	0.00	0.01	0.08	2.42
2	0.00	-0.03	0.09	2.10	0.00	-0.00	0.08	2.41
3	0.02	0.00	0.14	2.10	0.02	0.00	0.10	2.42
4	-0.02	0.00	0.14	2.10	-0.02	0.00	0.10	2.42
5	0.00	0.00	0.17	2.10	-0.00	-0.00	0.13	2.41
6	0.00	0.00	0.17	2.10	0.00	-0.00	0.13	2.42
7	0.00	0.00	0.17	2.10	0.00	-0.00	0.13	2.42
8	0.00	0.00	0.17	2.10	0.00	-0.00	0.13	2.41
9	-0.02	0.00	0.14	2.10	-0.02	0.00	0.10	2.42
10	0.02	0.00	0.14	2.10	0.02	0.00	0.10	2.42
11	0.00	-0.03	0.09	2.10	0.00	-0.00	0.08	2.41
12	0.00	0.03	0.09	2.10	0.00	0.01	0.08	2.42
13	0.00	0.00	0.05	1.91	0.00	0.00	0.04	1.96

opposite behavior, i.e. the orbital moments deviate away from the $z-$axis in the lower part of the cluster and they are directed towards the $z-$axis in the upper part. but we note that these deviations are not significantly above the numerical noise level. This becomes evident if one compares data for those atoms that are mutually equivalent (apart from rotations around the z-axis) by symmetry: 1-4, 5-8, 9-12. While the symmetry requirement is (almost) obeyed by the atoms 5-8, deviations of a few 1/100 μ_B are found between the

TABLE IV: Cluster averaged values for $\langle \mathrm{L} \rangle = \frac{1}{13}\sum_{i=1}^{13} |\mathbf{L}_i|$ and $\langle \mathrm{S} \rangle = \frac{1}{13}\sum_{i=1}^{13} |\mathbf{S}_i|$ of MT M_{13} clusters are shown in μ_B/atom, compared to bulk values for bcc Fe, fcc Co and Ni as obtained from our calculations.

Cluster	$\langle \mathrm{L} \rangle$	$\langle \mathrm{S} \rangle$	$\langle \lvert\mathbf{L}\rvert \rangle_{\mathrm{bulk}}$	$\langle \lvert\mathbf{S}\rvert \rangle_{\mathrm{bulk}}$
Fe_{13}	0.084	3.04	0.06	2.25
Co_{13}	0.125	2.08	0.08	1.67
Ni_{13}	0.070	0.66	0.05	0.65

TABLE V: The values of prefactors in the Heisenberg anisotropy term in Eq. (2) for the relaxed M_{13} clusters.

Cluster	D_2 (meV)	D_4(meV)	$D_6(\mu eV)$
Fe_{13} (ICO) (46 μ_B)	–	–	-41.1
Fe_{13} (JT) (44 μ_B)	15.2	–	–
Fe_{13} (MT) (44 μ_B)	–	-11.5	-41.1
Co_{13} (31 μ_B)	–	-21.7	-25.1
Ni_{13} (8 μ_B)	–	7.1	7.3

atoms 1-4 and also between the atoms 9-12.

When comparing the numerical results for spin and orbital magnetic moments from these two different calculational methods, one must take into acount the difference in their definition. In VASP, the properties (spin and orbital moments) are extracted as projection onto an atomic sphere (see Section II). The "standard" VASP value of atomic sphere radius for Co does in fact correspond to slightly overlapping spheres in our Co_{13} cluster. The SIESTA output results are reported in terms of decomposition over projection onto localized, but spatially extended, numerical orbitals, known as Mulliken population analysis. It is known that the local magnetic moments as well as atomic charges in heterogeneous systems do often come out very different, when estimated according to these two different schemes. In order to illustrate this effect, we give in the last column of Table III the values of spin moment, extracted from the SIESTA results. The fluctuations of these integrated values over apparently equivalent atoms are caused by the sparseness of the spatial grid with the step 0.078 Å, on which the summation of spin density has been done.

The $\langle \mathrm{L} \rangle$ and $\langle \mathrm{S} \rangle$ of Fe_{13}, Co_{13} and Ni_{13} clusters are compared with respect to bulk in Table IV. The orbital and spin moments for bulk systems are calculated with the equlibrium lattice constants of 2.832 Å (bcc Fe), 3.52 Å (fcc Co) and 3.523 Å (fcc Ni). The orbital and

spin magnetic moments of the elemental Fe, Co and Ni clusters are larger than the related bulk values. For example, in Ref [60] it was shown that in Ni clusters of up to 13 atoms, the average orbital moment $\langle \mathrm{L} \rangle$ per atom is found to be 4 to 8 times larger with respect to $\mathrm{L_{bulk}}$; for larger cluster sizes, $\langle \mathrm{L} \rangle$ was shown to approach the bulk value. It turns out from our calculation that for $\mathrm{Ni_{13}}$ clusters, $\langle \mathrm{L} \rangle$ agrees quite well with the earlier report [60], with orbital moment having larger magnitude than the bulk value. For $\mathrm{Fe_{13}}$ and $\mathrm{Co_{13}}$, the $\langle \mathrm{L} \rangle$ is also relatively large with respect to the bulk systems. In addition, the average spin moments $\langle \mathrm{S} \rangle$ for these clusters are also increased with respect to the bulk systems.

In addition, the magnetic anisotropy energy for $\mathrm{M_{13}}$ clusters was calculated. Bulk $3d$ metals show a tiny (cubic Fe, Co and Ni) MAE of $\sim$1 μeV. The tiny value in cubic systems is due to the high symmetry and it is expected that an ideal ICO exhibits a similarly small MAE. If the symmetry is broken, e.g., by tetragonal distortion of a cubic system, the MAE increases considerably (see for instance Ref. 61).

Figure 2 shows the ideal icosahedral cluster and the definition of the (x, z)-plane with angle θ for the magnetization directions used in our MAE calculations. The magnetic anisotropy energy is computed from the total energy as $\Delta E = E^{tot}(\theta) - E^{tot}(\theta = 0)$, $E^{tot}(\theta)$ being the θ-dependent total energy. The θ-dependent energy obtained from total energy calculations is compared with the anisotropy term of the extended Heisenberg model, defined as

$$H = -\sum_{i \neq j} J_{ij} \mathbf{S}_i \mathbf{S}_j + H_{\mathrm{ani}} + H_{\mathrm{dipolar}}, \tag{1}$$

where

$$H_{\mathrm{ani}} = -\sum_{n} \sum_{i}^{N} D_n (\mathbf{e}_i \cdot \mathbf{S}_i)^n. \tag{2}$$

The spin-spin and dipolar interactions are neglected, while comparing *ab-initio* total energy differences with the Heisenberg model.

In Eq. (2), n is the order of anisotropy (an even integer), $\mathbf{e}_i$ are the unit vectors of the atoms along the radial directions, $\mathbf{S}_i$ their spin moments and D is the anisotropy constant (of Néel-like model), which is assumed to be θ-independent. The second and fourth order contributions are constant from symmetry considerations of a ideal ICO. The anisotropy consists then mostly of a sixth order contribution, assuming that still higher orders are negligibly small. Figure 3 shows a comparison of energy differences of an ideal

Fe_{13} ICO obtained from *ab-initio* calculations to that of the Heisenberg model using a least-mean square fit to the *ab-initio* data. It is a delicate task to correctly determine energy contributions in the order of a few μeV/atom or below. To obtain meaningful results presupposes that the charge density is extremely well converged and still consistent with the symmetry of the system. A distortion of the symmetry might occur due to numerical fluctuations (which can to a limited extent be controlled by, e.g., the choice of energy cutoff and Fourier-grid) and to perturbations by the setup of the model system itself, e.g., due to the electrostatic interaction between periodic images of the supercell. Suitable settings can be found from the corresponding contributions to the forces, which depend on the ionic positions and the charge distribution as well. Consequently, the magnitude of the forces acting on all equivalent atoms should be nearly equal, which in our case, we have taken care that forces are not larger than 10^{-6} eV/Å. It is shown from model calculations of fcc Co clusters that the θ-dependence of magnetic anisotropy may also differ with the polar angle ϕ [62], which is not discussed here.

Along with the MAE for a ideal cluster shown in Fig. 3, the MAE of relaxed M_{13} clusters is calculated: The variation of energy difference with respect to θ for relaxed clusters are shown in Fig. 4. The θ-dependent energy difference for the JT-distorted Fe_{13} cluster (the top panel of Fig. 4) gives rise to a significant D_2 contribution of ~ 15.2 meV for the anisotropy. However, approximately only a D_4 and D_6 contribution arises for the anisotropy in case of MT Fe_{13} cluster. The values are depicted in Table V. The MAE for the JT-distorted Fe cluster is calculated to be 322 μeV/atom, which is approximately five times larger with respect to the MT cluster ($MAE_{MT} = 60$ μeV/atom). The reason behind the large MAE for the JT-distorted cluster relative to the MT cluster may be attributed to the breaking of symmetry in the former case.

The θ-dependent energy difference for the relaxed MT Fe_{13} cluster shows qualitatively good resemblance with that of the ideal cluster (see Fig. 3), however, the quantitative MAE value for ideal Fe_{13} ICO is found to be approximately 1 μeV/atom, while for the MT Fe_{13} cluster, it is approximately 60 times larger than for the ideal cluster. However, for relaxed geometries of Co_{13} and Ni_{13}, the MAE value is calculated to be 5 and 0.64 μeV/atom, respectively. Our calculations suggest a larger value of MAE per atom for Fe_{13} and Co_{13} compared to the bulk, which is 1.4 μeV/atom (bcc Fe), 1.3 μeV/atom (fcc Co) [63]. For Ni_{13},

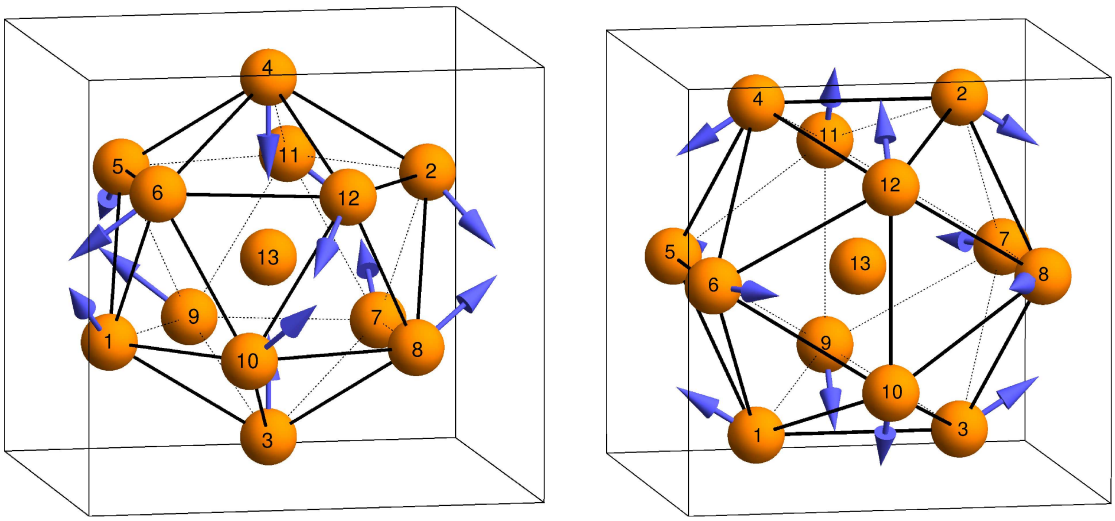

FIG. 1: The JT-distorted (left) and the MT (right) Fe_{13} cluster. Arrows indicate the direction of relative shift of atoms with respect to the ideal positions. For the JT-distorted and MT Fe_{13} cluster, the displacements marked by the arrows have been scaled up by a factor of 20 and 30, respectively. The box is only guide to the eyes. (The actual simulation box size is 15^3 Å^3.)

this is lower with respect to bulk fcc Ni (2.7 μeV/atom). The small anisotropy for the relaxed Ni_{13} cluster relative to bulk Ni is due to the high symmetry of the cluster, Ni_{13} having a nearly ideal icosahedral shape. The change of sign in the energy vs. θ-curves (shown in Fig. 4) for the relaxed M_{13} clusters can be explained through their way of structural relaxation. Namely, the MT relaxation pattern for the Co_{13} cluster is just opposite to that of Fe_{13}: The Co "dimers" oriented along the edges of the cube in the right panel of Fig. 1 make the shortest side in each Co_3 face, whereas the corresponding Fe-Fe bonds are the longest in the Fe_3 faces of the MT Fe_{13} cluster, see Table II. By comparing *ab-initio* results with the Heisenberg anisotropy term, the D_4 of M_{13} can be fitted, which are listed in Table V. It is observed that D_4 makes a significant contribution to the magnetic anisotropy of the relaxed clusters having cubic-like distortions.

It would be fascinating to see how spin and orbital moment as well as the MAE change, if we consider more "asymmetric" clusters. To this we have added a varying number of Pt atoms on the top of M_{13} clusters.

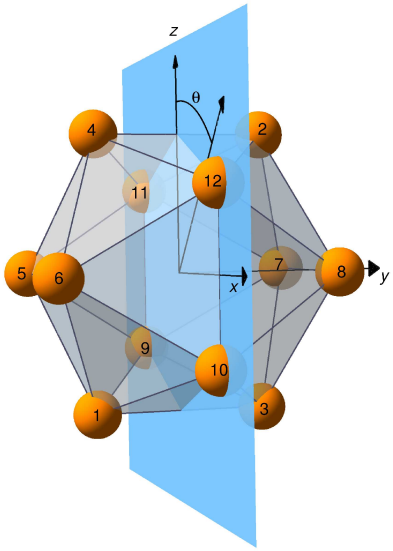

FIG. 2: The ideal icosahedral cluster showing the x-z plane in which the angle θ is varied in the MAE calculations for the partially Mackay transformed clusters.

IV. RESULTS FOR CAPPED CLUSTERS $M_{13}Pt_n$

Obviously, binary and core-shell transition metal clusters show a yet larger diversity compared to the elemental systems. For example, the intermixing of $3d$ elements with $4d$ or $5d$ elements results in a large magnetic moment of the binary systems [26]. Both in experiment and in calculations, it has been observed that FePt and Co clusters show enhanced spin moments and orbital moments with respect to corresponding bulk values [64, 65]. Hence, it would be interesting to study the change in magnetic properties including MAE of M_{13} clusters capping with Pt atoms, which is described in the following.

We considered three high-symmetry positions to cap the M_{13} clusters by a single Pt atom and found that a Pt position above the centre of a facet is most favorable in all three cases. In the following, we used this finding as a guideline for initial geometries of $M_{13}Pt_n$ clusters (n = 3, 4, 5, 20): In all cases, the Pt atoms were initially placed above the facet centres at a distance found in the single-Pt capping case. After relaxation, optimised geometries were obtained as shown in Fig. 5 for $Co_{13}Pt_3$ (left) and $Co_{13}Pt_5$ (right) and in Fig. 6 (right side) for $Ni_{13}Pt_{20}$. For n = 20, the initial geometries form a core-shell morphology.

Since atom projected quantities like spin and orbital moments depend on the specific code, we compared for the particular case of $Ni_{13}Pt_3$ related data obtained by VASP and

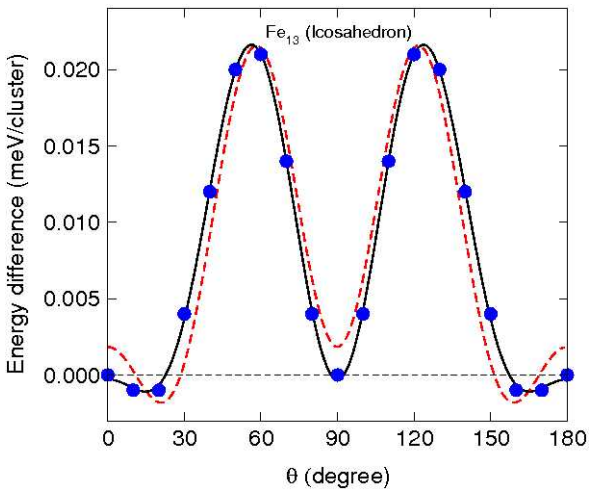

FIG. 3: The θ-dependent energy for an ideal Fe_{13} icosahedral cluster showing the *ab-initio* data (filled circles and solid line as guide to the eyes) compared with the Heisenberg model (dashed curve). For VASP calculations, the energy difference is in units of meV per cluster and is defined as $\Delta E = E - E_{\theta=0}$.

FPLO. The structure optimisation was carried out by VASP and the same geometry was used to evaluate the magnetic moments by both codes.

In FPLO, the magnetic moments are calculated through Mulliken population analysis. Figure 7 shows the absolute value of orbital moment per atom $|\mathbf{L}_i|$ (left) and the absolute value of spin moment per atom $|\mathbf{S}_i|$ (right) as a function of distance of each atom from the cluster centre for $Ni_{13}Pt_3$. It is obvious that both codes give results which are in good agreement with each other. Therefore, the calculations which are discussed in the following are done with VASP only.

In Figs. 8 and 9, the variation of $|\mathbf{L}_i|$ and of $|\mathbf{S}_i|$ with respect to the distance from centre of $M_{13}Pt_n$ clusters are shown, respectively (the symbols are kept consistent for both figures and the centre atom is placed at zero). Figure 8 nicely shows that the orbital moments of such few-atom systems in general depend very sensitively on the particular chemical composition and geometry. The resulting electronic structure can be very individual (e.g., the nature of the highest occupied level depends on the electron number and the spin moment) and is hard or impossible to predict without a detailed calculation. It is also found that (see Fig. 8) $|\mathbf{L}_i|$ for M_{13} clusters approach towards the corresponding bulk values of bcc Fe, fcc Co and Ni reported in Table IV, with increasing the number of Pt atoms. The orbital moment

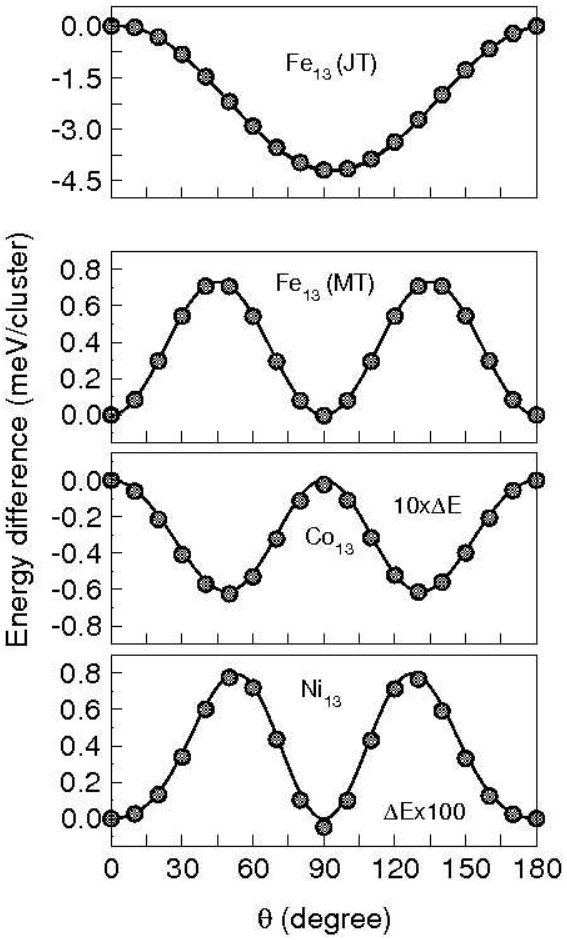

FIG. 4: The plots from top to bottom show the energy differences in meV/cluster vs. θ of relaxed Fe_{13} (for two types of relaxations - JT and Mackay distortion), Co_{13} and Ni_{13} clusters. In case of JT-distorted Fe_{13}: θ varies with respect to the z-axis in the plane passing through atom 4, middle of the bond between atoms 6-12, atom 10 and atom 3 (shown in the left side of Fig. 1), whereas for the MT cluster, θ varies through all atoms as depicted in Fig. 1. Energy difference is ($\Delta E = E - E_{\theta=0}$). The energy difference for the Co_{13} cluster is multiplied by a factor 10 and the energy difference for the Ni_{13} cluster is multiplied by a factor 100.

on the centre Fe atom for $Fe_{13}Pt_n$ cluster increases with the number of Pt atoms, whereas for $Co_{13}Pt_n$ and $Ni_{13}Pt_n$, this trend is weak. The orbital moment on Pt atoms is found to be very sensitive with respect to the core atomic species. For example, the $|\mathbf{L}_i|$ on Pt atoms for $Ni_{13}Pt_n$ clusters are enhanced relative to that of $Fe_{13}Pt_n$ and $Co_{13}Pt_n$.

In Fig. 9 the variation of spin moments for the capped clusters are shown, which suggests that with increasing Pt atoms, the $|\mathbf{S}_i|$ for M_{13} clusters always remain larger with respect

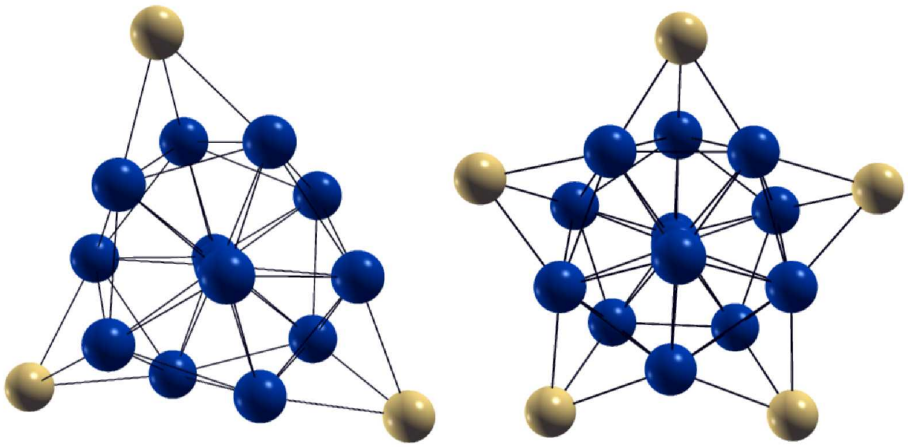

FIG. 5: The relaxed structure of $Co_{13}Pt_3$ (left) and $Co_{13}Pt_5$ (right) shows the arrangement of Pt atoms on the Co_{13} cluster, dark (blue) spheres: Co atoms and light (yellow) spheres: Pt atoms. In each case all Pt atoms lie in the same plane corresponding to the lowest energy structures found so far.

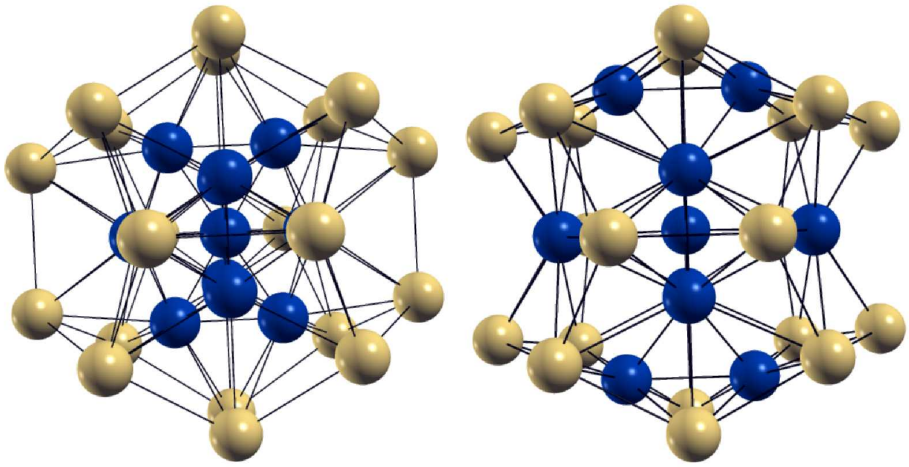

FIG. 6: The initial and final strucutres for the $Ni_{13}Pt_{20}$ cluster are shown in the left and right panel, respectively. Ni and Pt atoms are represented by dark (blue) and light (yellow) spheres, respectively. The final structure, corresponding to the lowest energy structure found so far, demonstrates the importance of atomic relaxations.

to the corresponding bulk $3d$-spin moments values. Unlike the trend in orbital moment, the spin moment on Pt atoms is not much affected by its core species. In the following, a few quantitative statements are made for each of the capped clusters.

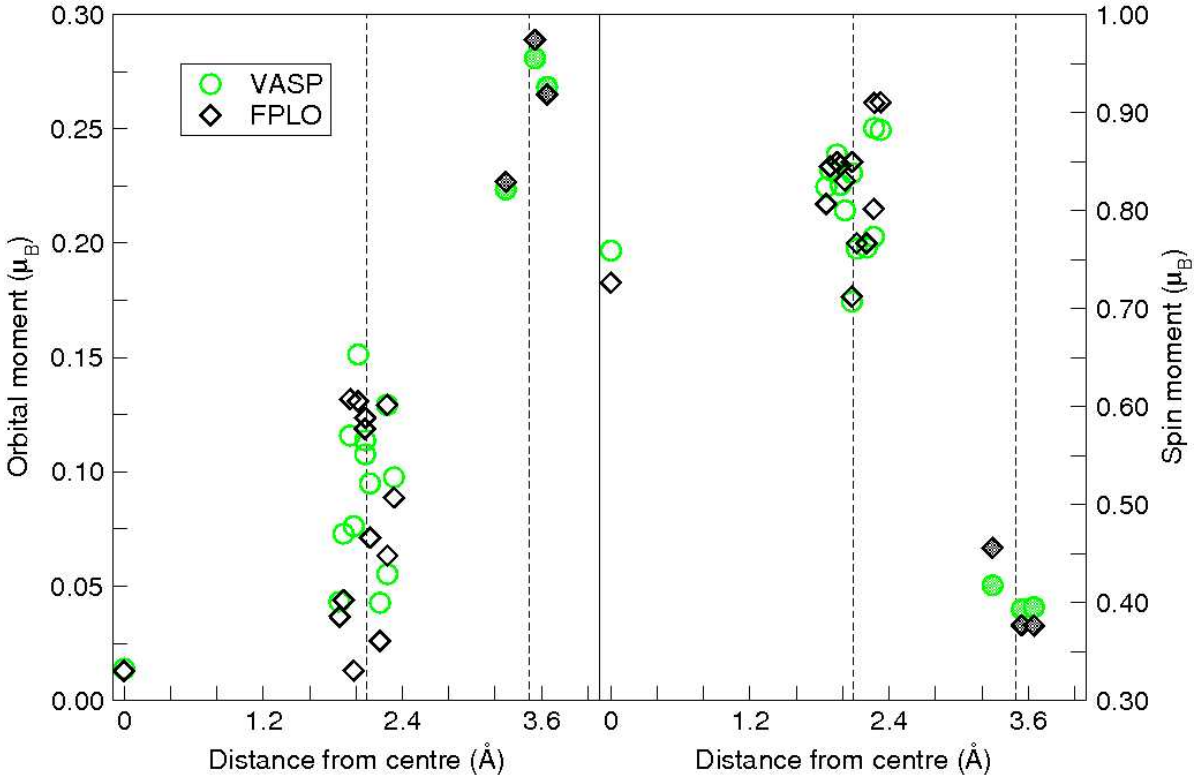

FIG. 7: The variation of the individual atomic $|\mathbf{L}_i|$ (left panel) and $|\mathbf{S}_i|$ (right panel) with respect to the distance from centre for $Ni_{13}Pt_3$ cluster. ◯: results by VASP and ♢: results by FPLO. The open and filled symbols (for both colors) show the moments on Ni and Pt atoms, respectively.

A. $Fe_{13}Pt_n$ clusters

The values of average orbital moment and average spin moment for each atomic species along with the total orbital moment L_{tot} and total spin moment S_{tot} for the capped clusters are defined and reported in Table VI. Our observation suggests that adding more Pt atoms on Fe_{13} cluster, the L_{tot} for $Fe_{13}Pt_n$ and S_{tot} for $Fe_{13}Pt_3$ and $Fe_{13}Pt_5$ increase considerably. However, there is a decrease of S_{tot} for $Fe_{13}Pt_{20}$ because of the antiferromagnetic like alignment of spin of centre Fe atom with respect to the sorrounding atoms in this cluster (for all other cappings, the Fe_{13} cluster is ferromagnetic). Capping with three and five Pt atoms enhances the atomic orbital moment on Fe_{13} by $\sim$ 50 % and 33 %, respectively, relative to the bulk value of bcc Fe, i.e. 0.06 μ_B/atom. It does not much change the Fe moment in comparison with the bare Fe_{13} cluster, however. The average orbital moment $\langle L_M \rangle$ on Fe_{13} decreases monotonically with increasing number of Pt atoms.

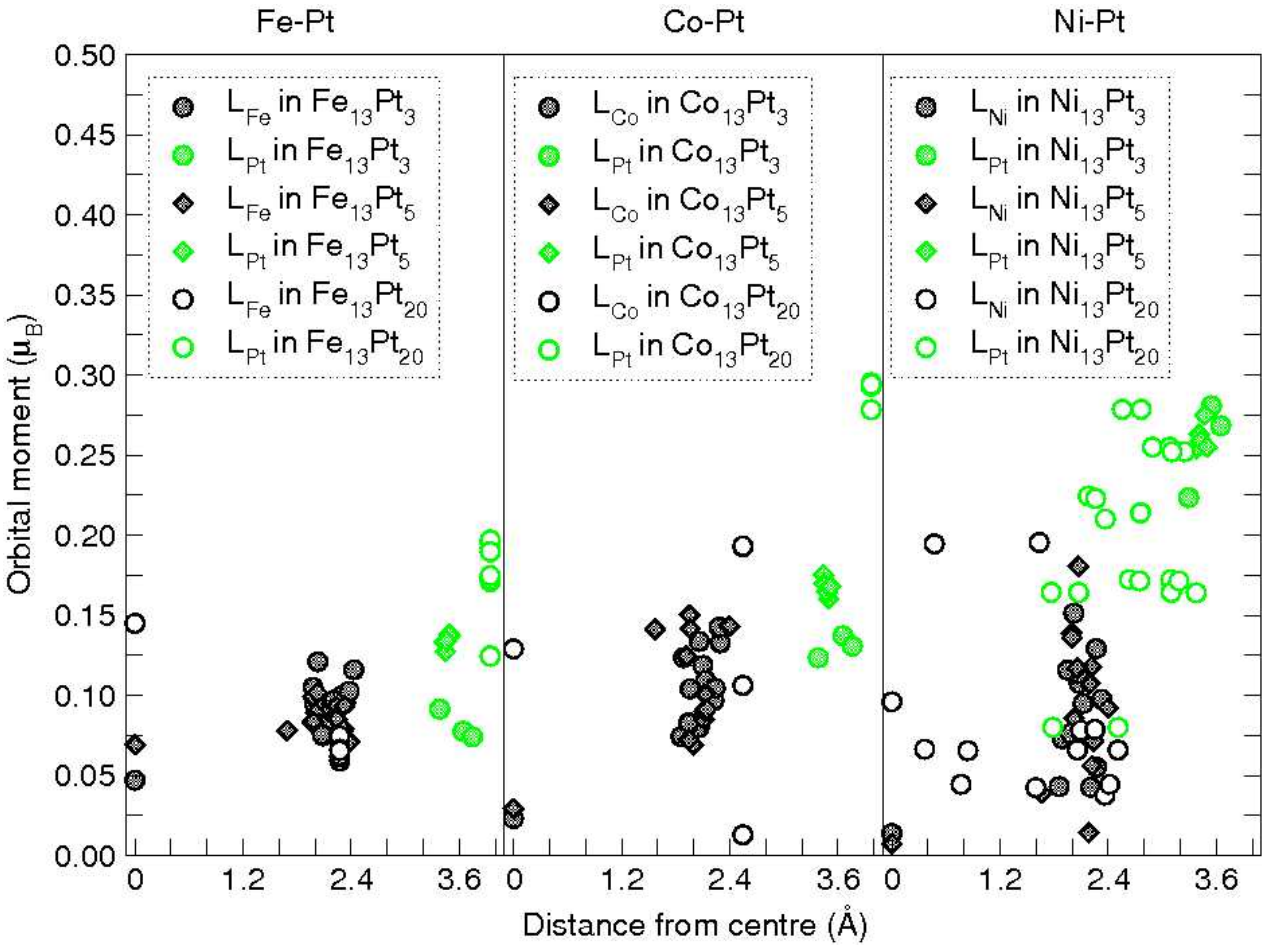

FIG. 8: The variation of the individual atomic orbital moments with respect to distance from centre for $Fe_{13}Pt_n$ (left), $Co_{13}Pt_n$ (middle) and $Ni_{13}Pt_n$ (right) clusters. The light (green) and dark (black) symbols for all cases represent the $|\mathbf{L}_i|$ on Pt atoms and M_{13} clusters, respectively.

B. $Co_{13}Pt_n$ clusters

A ferromagnetic ground state is found to be stable for all compositions of $Co_{13}Pt_n$ clusters, which leads to a monotonically increasing trend of L_{tot} and S_{tot} in these clusters. The $\langle L_M \rangle$ and $\langle L_{Pt} \rangle$ for $Co_{13}Pt_n$ clusters shows a trend similar to $Fe_{13}Pt_n$, i.e. with increasing number of Pt atoms, the $\langle L_M \rangle$ (as defined in Table VI) on the Co_{13} cluster decreases and the $\langle L_{Pt} \rangle$ on the Pt atoms is enhanced. The $\langle S_M \rangle$ on Co_{13} is merely constant, while it increases monotonically for Pt with more Pt atoms on the cluster surface.

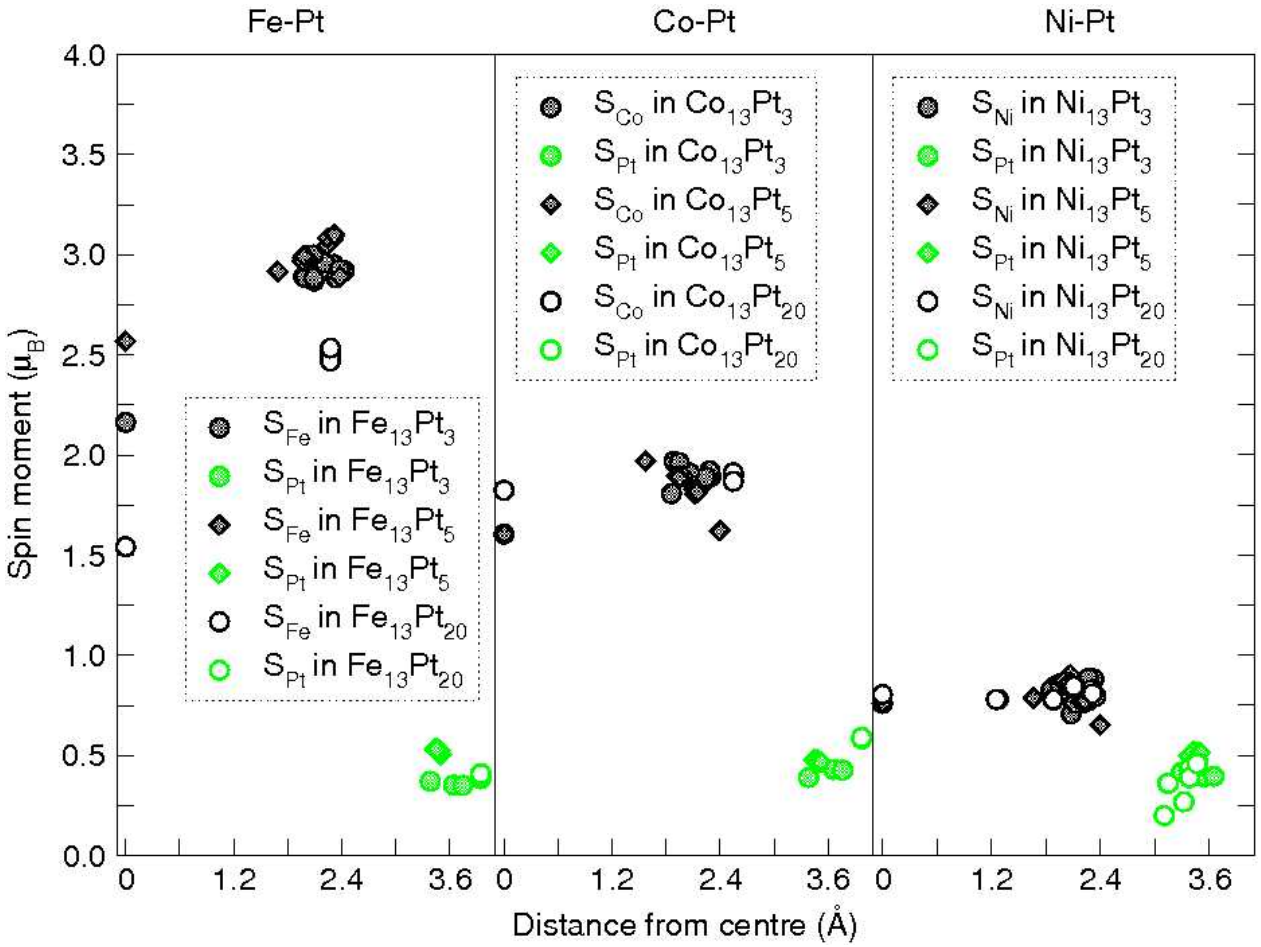

FIG. 9: The plots in the left, middle and right panels show the variation of $|\mathbf{S}_i|$ with respect to the distance from centre for $Fe_{13}Pt_n$, $Co_{13}Pt_n$ and $Ni_{13}Pt_n$ clusters, respectively. The same symbols are used here as in Fig. 8.

C. $Ni_{13}Pt_n$ clusters

In this case, the L_{tot} and S_{tot} also show a regular increase with the number of Pt atoms. The $\langle L_M \rangle$ and $\langle L_{Pt} \rangle$ for this cluster do not much depend on the number of Pt atoms. However, a decrease of $\langle L_{Pt} \rangle$ and $\langle S_{Pt} \rangle$ from $Ni_{13}Pt_5$ to $Ni_{13}Pt_{20}$ cluster is also observed. This is probably caused by a structural instability occuring for this composition upon the relaxation. The geometry optimization of this cluster converges to a structure with different symmetry, with a ferromagnetic ordering, where the Ni atoms are placed closer to the surface of the cluster as shown in Fig. 6. The reason for the segregation of Ni atoms towards the surface may be due to its lower surface energy compared to Pt [66]. Another aspect related

TABLE VI: The orbital and spin moments for the binary Pt-M clusters in μ_B/atom, where we have distinguished core and shell contributions. Cluster averaged values are defined for $\langle \mathrm{L_M} \rangle = \frac{1}{13}\sum_{i=1}^{13} |\mathbf{L}_i|$ and $\langle \mathrm{S_M} \rangle = \frac{1}{13}\sum_{i=1}^{13} |\mathbf{S}_i|$ (M represents the 13-atom Fe, Co and Ni clusters). The averaged values for $\langle \mathrm{L_{Pt}} \rangle = \frac{1}{n}\sum_{i=1}^{n} |\mathbf{L}_i|$ and $\langle \mathrm{S_{Pt}} \rangle = \frac{1}{n}\sum_{i=1}^{n} |\mathbf{S}_i|$ (n is the number of Pt atoms and here, n= 3, 5, 20). $|\mathbf{L_{tot}}|$ and $|\mathbf{S_{tot}}|$ are the corresponding absolute values of the total orbital and spin moment for every composition of the binary clusters.

Cluster	$\langle \mathrm{L_M} \rangle$	$\langle \mathrm{L_{Pt}} \rangle$	$\langle \mathrm{S_M} \rangle$	$\langle \mathrm{S_{Pt}} \rangle$	$\lvert\mathbf{L_{tot}}\rvert$	$\lvert\mathbf{S_{tot}}\rvert$
$Fe_{13}Pt_3$	0.09	0.08	2.86	0.36	1.43	38.3
$Fe_{13}Pt_5$	0.08	0.134	2.97	0.526	1.76	41.3
$Fe_{13}Pt_{20}$	0.05	0.17	2.18	0.401	2.74	36.4
$Co_{13}Pt_3$	0.1	0.13	1.87	0.42	1.68	25.6
$Co_{13}Pt_5$	0.095	0.16	1.83	0.47	2.06	26.1
$Co_{13}Pt_{20}$	0.07	0.3	1.88	0.60	4.9	36.2
$Ni_{13}Pt_3$	0.06	0.2	0.81	0.402	1.61	11.7
$Ni_{13}Pt_5$	0.05	0.26	0.80	0.512	2.01	13.0
$Ni_{13}Pt_{20}$	0.08	0.2	0.81	0.36	3.55	17.6

to this may be observed in the right panel of Figs. 8 and 9 showing the variation of onsite orbital and spin moments with respect to the distance. The large variations in orbital and spin moments just occur because of the structural distortion for this cluster composition. Comparing all three cases of capped clusters, we find that the presence of Pt atoms on M_{13} affects the orientation of core orbital moments in such a way that they always prefer to be in non-collinear alignment for the $M_{13}Pt_n$ clusters, which is not the case in the uncapped M_{13} clusters. On the other hand, directions of individual spin moments remain always collinear for the same clusters indicating that they are less affected by the Pt atoms.

Regarding the MAE of capped $M_{13}Pt_n$ clusters, we observe that the symmetry rules the magnitude of the effect like for M_{13} systems. For example, in $Fe_{13}Pt_4$ (see Fig. 10) with second-order anisotropy, we find a high MAE value, even larger by a factor of two ($\sim$ 7 meV/cluster) compared to JT-distorted Fe_{13}.

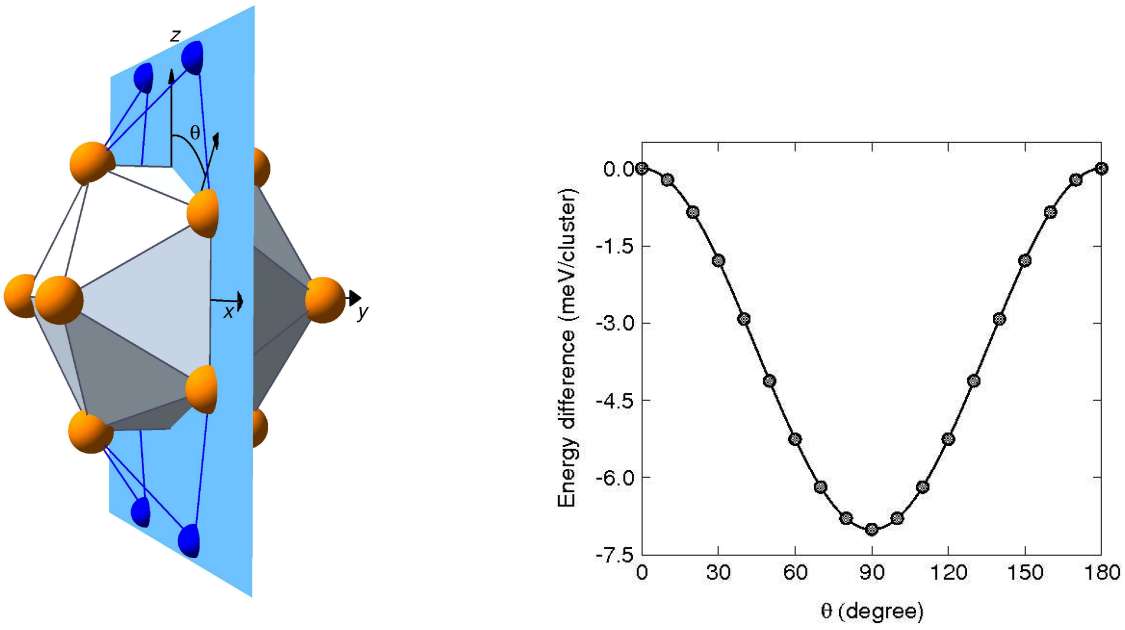

FIG. 10: Left: The x-z plane (where θ is varied) of the $Fe_{13}Pt_4$ cluster, showing the positions of the Pt-atoms relative to the ICO in the unrelaxed configuration. Light (orange) and dark (blue) spheres are the Fe and Pt atoms, respectively. Right: The θ-dependent energy differences for the relaxed $Fe_{13}Pt_4$ cluster. The energy difference is in units of meV per cluster and is defined as $\Delta E = E - E_{\theta=0}$.

V. CONCLUSION

The spin and orbital magnetic moments are calculated for M_{13} and $M_{13}Pt_n$ clusters including spin-orbit interaction using DFT methods. The studies on MAE of M_{13} clusters show that the calculated MAE values of relaxed M_{13} clusters are considerably enhanced relative to both the ideal icosahedral clusters and to the corresponding bulk values in case of Fe_{13} and Co_{13}. For Ni_{13}, the MAE is smaller than that of the bulk value of fcc Ni. The MAEs for relaxed clusters are found to be affected by the degree of relaxation due to which Fe_{13} clusters have a high anisotropy in comparison with Co_{13} and Ni_{13}. Iron is a special case for which we obtain two local energy minima [12, 56], corresponding to the JT and MT cases. The JT-distorted Fe_{13} cluster exhibits an anisotropy approximately 5 times larger than the partially MT cluster due to the low symmetry in the former case. The present calculations of MAE agree well with the qualitative prediction of the Heisenberg model for the θ-dependent energy differences. With respect to the spin and orbital moments, both the

capped and the free clusters show an increased value of orbital and spin moments compared to the bulk. For the capped clusters, the spin moments on Pt atoms remain unaffected by the host atoms. Finally, we infer that deposited transition metal clusters, with very large effects of relaxations, may even exhibit larger MAE values. Self-assembly of such clusters, like in case of Fe-Pt [13] and Co [14], may then approach the class of functional magnetic materials of use for magnetic storage devices.

Acknowledgments

The authors would like to acknowledge Helmut Eschrig and Klaus Koepernik for helpful discussions. This work was supported by SFB 445 and SPP 1145.

---

[1] S. Polesya, O. Šipr, S. Bornemann, J. Minár, and H. Ebert, Europhys. Lett. **74**, 1074 (2006).

[2] O. Šipr, S. Polesya, J. Minár, and H. Ebert, J. Phys.: Condens. Matter. **19**, 446205 (2007).

[3] Y. Xie, and J. A. Blackman, Phys. Rev. B **66**, 085410 (2002).

[4] O. Dièguez, M. M. G. Alemay, C. Rey, P. Ordejón, and L. J. Gallego, Phys. Rev. B **63**, 205407 (2001).

[5] A. V. Postnikov, P. Entel, and J. M. Soler, Eur. Phys. J. D **25**, 261 (2003).

[6] H. M. Duan and Q. Q. Zheng, Phys. Lett. A **280**, 333 (2001).

[7] S. E. Apsel, J. W. Emmert, J. Deng, and L. A. Bloomfield, Phys. Rev. Lett. **76**, 1441 (1996).

[8] B. J. Winter, T. D. Klots, E. K. Parks, and S. J. Riley, Z. Phys. D **19**, 375 (1991); J.-O. Bovin, and J.-O. Malm, Z. Phys. D **19**, 293 (1991).

[9] B. I. Dunlap, Phys. Rev. A **41**, 5691 (1990).

[10] M. L. Tiago, Y. Zhou, M. M. G. Alemany, Y. Saad, and J. R. Chelikowsky, Phys. Rev. Lett. **97**, 147201 (2006).

[11] P. Entel, M. E. Gruner, G. Rollmann, A. Hucht, S. Sahoo, A. T. Zayak, H. C. Herper, A. Dannenberg, Phil. Mag. **88**, 2725 (2008).

[12] G. Rollmann, M. E. Gruner, A. Hucht, R. Meyer, P. Entel, M. L. Tiago, and J. R. Chelikowsky, Phys. Rev. Lett. **99**, 083402 (2007).

[13] M. E. Gruner, G. Rollmann, P. Entel, and M. Farle, Phys. Rev. Lett. **100**, 087203 (2008).

[14] Xiao *etal.*, http://arxiv.org/abs/0906.4645.

[15] T. Futschek, J. Hafner, and M. Marsman, J. Phys.: Condens. Matter, **18**, 9703 (2006).

[16] L. M. Sandratskii, Adv. Phys. **47**, 91 (1998).

[17] L. M. Sandratskii, and J. Kübler, Mod. Phys. Lett. B **10**, 189 (1996).

[18] T. Oda, A. Pasquarello, and R. Car, Phys. Rev. Lett. **80**, 3622 (1998).

[19] D. Hobbs, G. Kresse, and J. Hafner, Phys. Rev. B **62**, 11556 (2000).

[20] S. Lounis, P. Mavropoulos, R. Zeller, P. Dederichs, and S. Blügel, Phys. Rev. B **75**, 174436 (2007).

[21] T. O. Strandberg, C. M. Canali, and A. H. MacDonald, Nature Mater. **6**, 648 (2007).

[22] P. Gambardella, S. Rusponi, M. Veronese, S. S. Dhesi, C. Grazioli, A. Dallmeyer, I. Cabria, R. Zeller, P. H. Dederichs, K. Kern, C. Carbone, and H. Brune, Science **300**, 1130 (2003).

[23] F. Luis, J. Bartolomé, M. J. Martinez, and L. M. Garcia, J. Appl. Phys. **99**, 08G705 (2006).

[24] J. Bansmann, S. H. Baker, C. Binns, J. A. Blackman, J.-P. Bucher, J. Dorantes-Dávila, V. Dupuis, L. Favre, D. Kechrakos, A. Kleibert, K.-H. Meiwes-Broer, G. M. Pastor, A. Perez, O. Toulemonde, K. N. Trohidou, J. Tuaillon, and Y. Xie, Surf. Sci. Rep. **56**, 189 (2005).

[25] S. Dennler, J. Morillo, and G. M. Pastor, J. Phys.: Condens. Matter. **16**, S2263 (2004).

[26] M. Muñoz-Navia, J. Dorantes-Dávila, and G. M. Pastor, J. Phys.: Condens. Matter. **16**, S2251 (2004).

[27] M. Tsujikawa, A. Hosokawa, and T. Oda, Phys. Rev. B **77**, 054413 (2008).

[28] R. Félix-Medina, J. Dorantes-Dávila, and G. M. Pastor, Phys. Rev. B **67**, 094430 (2003).

[29] B. Nonas, I. Cabria, R. Zeller, and P. H. Dederichs, Phys. Rev. Lett. **86**, 2146 (2001).

[30] A. N. Andriotis, and M. Menon, Phys. Rev. Lett. **93**, 026402 (2004).

[31] S. Rohart, C. Raufast, L. Favre, E. Bernstein, E. Bonet, and V. Dupuis, Phys. Rev. B **74**, 104408 (2006).

[32] M. Tsujikawa, A. Hosokawa, and T. Oda, Phys. Rev. B **77**, 054413 (2008).

[33] S. Pick, V. S. Stepanyuk, A. L. Klavsyuk, L. Niebergall, W. Hergert, J. Kirschner, and P. Bruno, Phys. Rev. B **70**, 224419 (2004).

[34] G. M. Pastor, J. Dorantes-Dávila, S. Pick, and H. Dreysse, Phys. Rev. Lett. **75**, 326 (1995).

[35] L. Fernández-Seivane, and J. Ferrer, Phys. Rev. Lett. **99**, 183401 (2007).

[36] J. Hong, and R. Q. Wu, J. Appl. Phys. **69**, 6147 (1991).

[37] D. Fritsch, K. Köpernik, M. Richter, and H. Eschrig, J. Comp. Chem. **29**, 2210 (2008).

[38] P. Błoński and J. Hafner, Phys. Rev. B **79**, 224418 (2009).

[39] O. Diéguez, M. M. G. Alemany, C. Rey, P. Ordejon, and L. J. Gallego, Phys. Rev. B **63**, 205407 (2001).

[40] G. Kresse, and J. Furthmüller, Comput. Mater. Sci. **6**, 15 (1996),

[41] G. Kresse, and J. Furthmüller, Phys. Rev. B **54**, 11169 (1996),

[42] G. Kresse, and D. Joubert, Phys. Rev. B **59**, 1758 (1999).

[43] J. M. Soler, E. Artacho, J. D. Gale, A. Gracia, J. Junquera, P. Ordejon, and D. Sanchez-Portal, J. Phys.: Condens. Matter **14**, 2745 (2002).

[44] K. Koepernik and H. Eschrig, Phys. Rev. B **59**, 1743 (1999).

[45] J. P. Perdew, in *Electronic Structure of Solids'91,* edited by P. Ziesche and H. Eschrig (Berlin, Akademie Verlag, 1991), pp. 11-20.

[46] P. E. Blöchl, Phys. Rev. B **50**, 17953 (1994).

[47] J. P. Perdew, K. Burke, and M. Ernzerhof, Phys. Rev. Lett. **77**, 3865 (1996).

[48] N. Troullier and J. L. Martins, Phys. Rev. B **43**, 1993 (1991).

[49] J. Junquera, O. Paz, D. Sanchez-Portal, and E. Artacho, Phys. Rev. B **64**, 235111 (2001).

[50] L Fernandez-Seivane, M. A. Oliveira, S. Sanvito and J. Ferrer, J. Phys.: Condens. Matter **18**, 7999 (2006).

[51] http://www.fplo.de/

[52] J. P. Perdew and Y. Wang, Phys. Rev. B **45**, 13244 (1992).

[53] H. Eschrig, M. Richter, and I. Opahle, in: *Relativistic Solid State Calculations. Relativistic Electronic Structure Theory – Part II: Applications*, edited by P. Schwerdtfeger (Amsterdam: Elsevier, 2004), pp. 723-776.

[54] G. Rollmann, S. Sahoo, and P. Entel, Phys. Stat. Solidi (A) **201**, 3263 (2004).

[55] G. Rollmann, P. Entel, and S. Sahoo, Comput. Matter. Sci. **35**, 275 (2006).

[56] G. Rollmann, Ph.D. Thesis, University of Duisburg-Essen (2007).

[57] A. L. Mackay, Acta Cryst. **15**, 916 (1962).

[58] H. A. Jahn and E. Teller, Proc. R. Soc. London A **161**, 220 (1937).

[59] P. Entel, M. E. Gruner, A. Hucht, R. Meyer, G. Rollmann, S. Sahoo, and S. K. Nayak, in: *Mesoscopic, Nanoscopic and Macroscopic Materials*, edited by S. M. Bose, S. N. Behera, and B. K. Roul, AIP Conf. Proc. 1063, 3 (2008), pp. 3-17

[60] R. A. Guirado-López, J. Dorantes-Dávila, and G. M. Pastor, Phys. Rev. Lett. **90**, 226402

(2003).

[61] M. E. Gruner, P. Entel, I. Opahle, and M. Richter, J. Mater. Sci. **43**, 3825 (2008).

[62] R Yanes, and O Chubykalo-Fesenko, J. Phys. D: Appl. Phys. **42**, 055013 (2009).

[63] S. V. Halilov, A. Ya. Perlov, P. M. Oppeneer, A. N. Yaresko, and V. N. Antonov, Phys. Rev. B **57**, 9557 (1998).

[64] H. G. Boyen, K. Fauth, B. Stahl, P. Ziemann, G. Kästle, F. Weigl, F. Banhart, M. Hessler, G. Schütz, N. S. Gajbhiye, J. Ellrich, H. Hahn, M. Büttner, M. G. Garnier, and P. Oelhafen, in: Verhandl. DPG (VI), **39**, 1/ 253 (2004).

[65] H. Ebert, S. Bornemann, J. Minár, P. H. Dederichs, R. Zeller, and I. Cabria, Comput. Matter. Sci. **35**, 279 (2006).

[66] J. A. Alonso and N. H. March, *Electrons in Metals and Alloys* (Academic, London, 1989), pp. 433-444.